Theoretical fluorescence induction curves derived from coupled differential equations describing the primary photochemistry of photosystem II by an exciton–radical pair equilibrium

H.-W. Trissl, Y. Gao, and K. Wulf
Abt. Biophysik, Fachbereich Biologie/Chemie, Universität Osnabrück, D-4500 Osnabrück, Germany

ABSTRACT Fluorescence induction curves were calculated from a molecular model for the primary photophysical and photochemical processes of photosystem II that includes reversible exciton trapping by open (PHQ_A) and closed (PHQ_A^-) reaction centers (RCs), charge stabilization as well as quenching by oxidized ($P^+HQ_A^{(-)}$) RCs. For the limiting case of perfectly connected photosynthetic units ("lake model") and thermal equilibrium between the primary radical pair (P^+H^-) and the excited singlet state, the primary reactions can be mathematically formulated by a set of coupled ordinary differential equations (ODE). These were numerically solved for weak flashes in a recursive way to simulate experiments with continuous illumination. Using recently published values for the molecular rate constants, this procedure yielded the time dependence of closed RCs as well as of the fluorescence yield (= fluorescence induction curves). The theoretical curves displayed the same sigmoidal shapes as experimental fluorescence induction curves. From the time development of closed RCs and the fluorescence yield, it was possible to check currently assumed proportionalities between the fraction of closed RCs and either (*a*) the variable fluorescence, (*b*) the complementary area above the fluorescence induction curve, or (*c*) the complementary area normalized to the variable fluorescence. By changing selected molecular rate constants, it is shown that, in contrast to current beliefs, none of these correlations obeys simple laws. The time dependence of these quantities is strongly nonexponential. In the presence of substances that quench the excited state, the model predicts straight lines in Stern–Volmer plots. We further conclude that it is impossible to estimate the degree of physical interunit energy transfer from the sigmoidicity of the fluorescence induction curve or from the curvature of the variable fluorescence plotted versus the fraction of closed RCs.

INTRODUCTION

When the electron transport chain between photosystem II (PS II)[1] and photosystem I (PS I) is blocked, the fluorescence yield increases several times. Since the early years of photosynthesis research, this effect, which originates in PS II, has attracted continuous experimental and theoretical attention (for reviews see references 1–4). Quite recently, a rather detailed picture of the primary molecular processes of trapping, charge separation, and charge stabilization in PS II has emerged: the reversibility of these reactions has been established and the reactions have been described by an exciton–radical pair model (5–10).

Two reversible steps are to be considered: a photophysical and a photochemical. "Photophysical reversibility" means that once the primary donor is in the excited state, it can either initiate the primary charge separation or transfer the excitation energy back to antenna pigments. Whereas the charge separation occurs in 3 ps (11, 12), the single-step exciton transfer time may lie in the subpicosecond time regime (13–16). Hence, the exchange of excitation energy between all pigments of the antenna system occurs so rapidly that an equilibration of the excitation energy may be established in times much shorter than the charge stabilization time. A value of <15 ps has been reported for this process (17). In this case the primary charge separation becomes the rate-limiting step (trap-limited energy conversion).

"Photochemical reversibility" means that the radical pair, $P\text{-}680^+Phe^-$, formed by the primary photochemistry can recombine into the excited state with a high quantum yield (5–9). The forward and backward rate constants have been found to depend on the redox state of the first stable quinone acceptor (Q_A) (9) and also on the membrane potential (9, 18, 19). This explains on a molecular level the origin of the fluorescence increase when the acceptor site is blocked. By means of time-resolved fluorescence, absorption spectroscopy, and photovoltage measurements, the molecular rate constants of photosynthetic units (PSU) containing either open or closed reaction centers (RCs) (Q_A and Q_A^-, respectively) have been quantified or, at least, restrained (6, 8, 9, 20).

The distance over which an exciton can travel exceeds the physical size of a PSU. There is wide agreement that >3–5, perhaps even >20, RCs of PS II share a common antenna, termed "domain" (21 and references therein). This is practically indistinguishable from a perfect lake model organization (also termed "matrix," "multicentral," or "statistical" model) (3, 10, 21). The interunit energy transfer in the grana of chloroplasts may occur laterally and between at least two appressed membranes (22).

Out of the manifold of known fluorescence phenomena, we want to focus here on those occurring on a slow time scale. In experiments in which the electron transport is blocked after Q_A by herbicides (mostly 3-(3,4-

Address correspondence to Dr. H.-W. Trissl, Abteilung Biophysik, Fachbereich Biologie/Chemie, Universität Osnabrück, Barbarastrasse 11, D-4500 Osnabrück, Germany.

[1] *Abbreviations used in this paper:* chl, chlorophyll; DNB, *m*-dinitrobenzene; ODE, ordinary differential equation; PS I and PS II, photosystem I and II; PSU, photosynthetic unit; Q_A, first stable quinone acceptor; RC, reaction centers.

0006-3495/93/04/974/15 $2.00

dichlorophenyl)-1,1-dimethylurea) and a continuous light source is switched on, fluorescence increases in a sigmoidal way, yielding fluorescence induction curves. These can be simulated theoretically by rate equations if a lake model organization of the antenna system is assumed. However, two populations of states (open or closed units) and two sets of ordinary differential equations (ODE) with different rate constants have to be assumed and connected in an appropriate manner to account for the intermediate mixed states.

In the present article we inspect the exciton–radical pair model for its predictions of fluorescence induction phenomena. For particular sets of rate constants and different concentrations of the initial states, we calculate the time courses of fluorescence, radical pair formation (i.e., trapping time), and quinone reduction for delta function excitation of open and closed RCs. To simulate continuous light excitation and fluorescence induction curves, we solve the two sets of ODE in a recursive manner. This yields a new pseudo–time base, on which the closure of RCs and the increase of fluorescence (e.g., variable fluorescence) develops. These results then allow us to correlate the variable fluorescence as well as the so-called complementary area above the fluorescence induction curve with the fraction of closed RCs.

RESULTS

Description of the model

In the case of dark-adapted chloroplasts, the primary reactions in PS II after absorption of a photon may be described by the migration of excitation energy through antenna pigments (A_i) and primary donors, the reversible formation of a radical pair ($P^+H^-Q_A$), and the subsequent charge stabilization on a plastoquinone ($P^+HQ_A^-$). Thereafter, P^+ is reduced on a submicrosecond time regime by the secondary donor (Z), which yields the closed state (PHQ_A^-). Subsequently arriving excitons find a mixture of open (PHQ_A) and closed (PHQ_A^-) RCs. The interaction of excitons with closed RCs leads to the transient formation of a radical pair that decays either into the ground state or back reacts to form the excited state again.

The corresponding reaction scheme is shown in Fig. 1, *top*. The rate constants have the following meaning: k_t, for conversion of the excited state into the radical pair state (trapping rate constant); k_{-1}, for the back reaction; k_2, for charge stabilization; k_l, for monomolecular losses in the antenna system; and k_r, for the recombination of the radical pair into the ground state. The latter is assumed to be independent of the redox state. The superscript "ox" is used for RCs containing Q_A and "red" for RCs containing Q_A^-. The excitation energy, z_0, is expressed as the dimensionless quantity: absorbed photons per PSU and flash. Its time development, $z(t)$, describes the decay of the excited state.

With the basic assumptions of a lake model and a perfect equilibration within a homogeneous antenna system, the scheme can be described mathematically by the set of ODEs that is shown in Fig. 1, *bottom*. All concentrations of states, except z_0 and $z(t)$, refer to one PSU and consequently adopt values between 0 and 1 only. The conversion from all open to all closed RCs corresponds to exactly one redox equivalent.

The quenching of the oxidized primary donor, P-680$^+$ (23, 24), is accounted for by the term $k_c(B + C + E)z$ in the set of ODEs (Fig. 1). Its quenching rate constant was fixed at $(1\ \text{ns})^{-1}$.

The rate constant k_3 in Fig. 1 accounts for the transition from open to closed RC. It may stand for either the fast ns-formation of the (P-680 Q_A^-) state containing the oxidized secondary donor, Z^+, or the slower ms-formation of the (P-680 Q_A^-) state containing a mixture of redox states of the water-splitting enzyme (S states). However, this rate constant is not used in the present numerical calculations, since the transition from open to closed RC is realized by calculating the starting condition for the integration of the set of ODEs in a recursive way (for a more detailed description see below).

Choice of rate constants

Two laboratories have published numerical values of the molecular rate constants of the exciton–radical pair model of PS II (Table 1). The values reported by Schatz et al. (7, 8) were obtained from a reaction center preparation from a cyanobacterium containing 60–80 Chl/RC using the single-photon–timing fluorescence method. The values reported by Leibl et al. (9) were obtained from PS II-enriched membrane fragments (a so-called BBY-preparation[2] from peas) containing ~200 Chl/RC using a photoelectric method. (Parameter set no. 2 contains the numbers given by Leibl et al. (9) for the case of low ionic strength.) However, most studies on fluorescence induction are performed with chloroplasts of higher plants or whole algae, in which the antenna size of PS II may be larger, most likely near N = 250 (25). For modeling chloroplast data, we have chosen a further parameter set that was obtained for PS II_α centers from pea chloroplast with the single-photon–timing fluorescence technique (20) (Table 1, parameter no. 3).

Flash excitation

The set of ODEs was solved numerically for the time dependence of the states by a program that used the Runge–Kutta algorithm with a constant step width of 0.008 ns. Smaller stepwidths did not improve the results. The calculation was carried out to 8.192 ns, when all states have reached a steady-state level (step-to-step relative variations of the states of $<10^{-7}$). The starting con-

[2] After the researchers D. A. Berthold, G. Babcock, and C. F. Yocum, in 1981. See *FEBS (Fed. Eur. Biochem. Soc.) Lett.* 134:231–234.

open RCs:

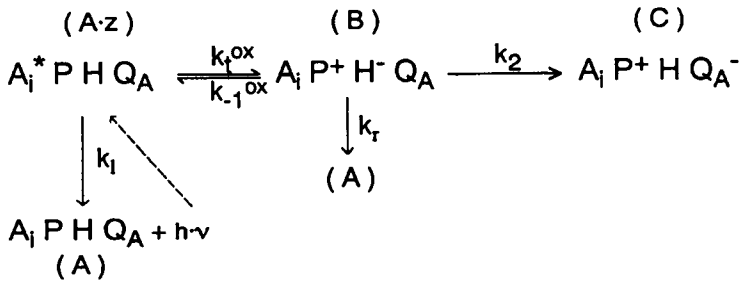

closed RCs:

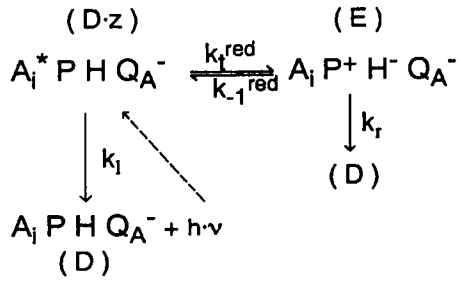

System of coupled differential equations:

$$1.\ \frac{dz}{dt} = -k_t^{ox}Az + k_{-1}^{ox}B - k_l z - k_c(B + C + E)z - k_t^{red}Dz + k_{-1}^{red}E$$

$$2.\ \frac{dB}{dt} = k_t^{ox}Az - k_{-1}^{ox}B - k_2 B - k_r B$$

$$3.\ \frac{dC}{dt} = k_2 B - k_3 C$$

$$4.\ \frac{dD}{dt} = k_3 C - k_t^{red}Dz + k_{-1}^{red}E + k_r E$$

$$5.\ \frac{dE}{dt} = k_t^{red}Dz - k_{-1}^{red}E - k_r E$$

with $A + B + C + D + E = 1$

FIGURE 1 Reaction scheme and set of ordinary differential equations.

dition was a flash of $z_0 = 0.05$ given to a system defined by $A(t = 0) = 1$ and $C(t = 0)$ (all RC open).

The decay of the excited state, $z(t)$, and the time developments of the radical pair, $B(t)$, and the charge stabilized state, $C(t)$, on exitation with a δ-function flash of an energy of $z_0 = 0.05$ for a system with initially 100% open RCs are shown in Fig. 2, *a* and *b*, using parameter set no. 1 and 2, respectively. A lag phase, typical for

TABLE 1 List of molecular time constants, τ_i [ns] ($\tau_i = k_i^{-1}$; defined in Fig. 1) for the primary reactions of PS II in the open and closed state

Parameter set no.	Reference	τ_l	Open (Q_A) τ_t^{ox}	Open (Q_A) τ_{-1}^{ox}	Open (Q_A) τ_2	Closed (Q_A^-) τ_t^{red}	Closed (Q_A^-) τ_{-1}^{red}	Φ_p	F_o	F_m	F_v	F_m/F_o	F_a	F_a/F_v
1	Schatz et al. (8)	1	0.11	0.50	0.50	0.67	0.42	0.80	1.00	5.45	4.45	5.44	5.42	1.22
2	Leibl et al. (9)	1	0.52	2.50	0.51	1.56	0.33	0.60	2.14	5.50	3.36	2.57	5.44	1.62
3	Roelofs et al. (20)	3.3	0.33	3.33	0.44	2.13	2.94	0.89	1.83	8.39	6.56	4.59	10.3	1.57

Calculated values for the photochemical quantum yield, Φ_p; the fluorescence yield, F_o; the fluoresence yield, F_m; the variable fluorescence, F_v; the ratio of fluorescence yields for open and closed states, F_m/F_o; the complementary area, F_a; and the complementary area normalized to the variable fluorescence, F_a/F_v. The fluorescence yields, F_o and F_m, are abolute quantum yields expressed in %.

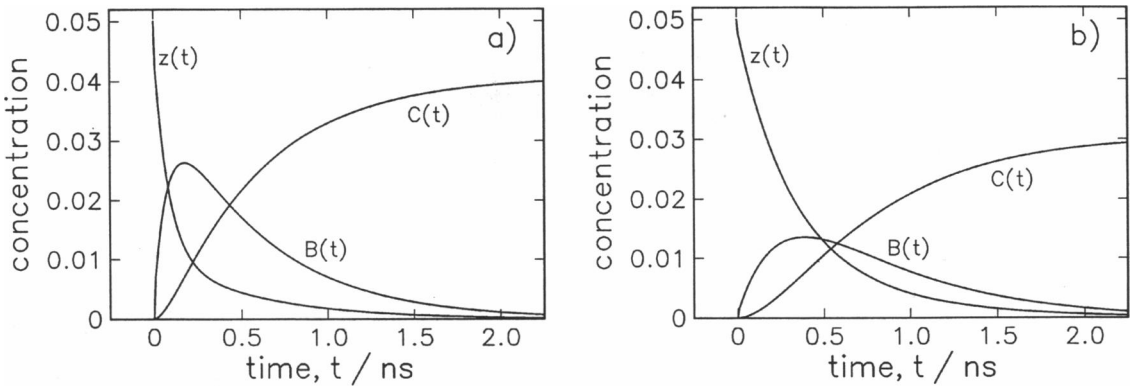

FIGURE 2 Time course of the excited state, $z(t)$, the radical pair, $B(t)$, and the charge stabilized state, $C(t)$, after excitation with a δ-function flash of an energy of $z_0 = 0.05$. Parameter set no. 1 (a) and no. 2 (b).

consecutive reactions, becomes apparent in the picosecond time regime of $C(t)$.

Both parameter sets yield rather similar picosecond kinetics, although differences are noticeable (Fig. 2). Evident is the higher maximal transient yield of the radical pair (which reaches almost 50% of z_0) and the higher yield of closed RC, $C(t \rightarrow \infty)$, for the parameter set of Schatz et al. (8) as compared with that for the one of Leibl et al. (9) (Fig. 2, a and b).

The photochemical quantum yield, Φ_p, follows from

$$\Phi_p = C(t \rightarrow \infty)/z_0. \quad (1)$$

The relative fluorescence yield is proportional to the time integral of $z(t)$:

$$\Phi_{fl} \sim \int_0^\infty z(t)\, dt. \quad (2)$$

Absolute fluorescence yields were obtained by normalizing this integral to that calculated for a system in which fluorescence is the only decay path. For the corresponding calculation, we have used a radiative lifetime of Chl a of 18 ns.

The fluorescence yield calculated for a system with all RCs initially open is called F_o and with all RCs initially closed F_m. The resulting ratios F_m/F_o for the three parameters sets are listed in Table 1.

Fluorescence induction curves

The progressive conversion from the open to the closed state was calculated by applying successive flashes of energy $z_i = 0.05$. The set of ODEs was solved in a recursive way for different initial conditions in which the result of the i − 1th flash $C_{i-1}(t \rightarrow \infty)$ is used as the starting condition for the ith flash. Hence, the starting condition of the ith flash reads $A_i(t = 0) = 1 - \sum C_{i-1}(t \rightarrow \infty)$ and $D_i(t = 0) = \sum C_{i-1}(t \rightarrow \infty)$. Smaller increments than $z_i = 0.05$ did not lead to a significant improvement in the results. The progression in z, $\sum z_i$, yields a new pseudo-time base, T:

$$T = \sum_{j=1}^{i} z_j, \quad (3)$$

which may be taken as the milli- or second time base in real fluorescence induction measurements. With this new time base, the absolute fluorescence in percent yield reads:

$$\Phi_{fl}(T) = c \cdot \sum_{j=1}^{i} \int_0^\infty z_j(t)\, dt, \quad (4)$$

with $i = T/z_0$ and $c = 1/(z_0 \cdot 0.18\ \text{ns})$. The fluorescence yield with all open and all closed RCs are consequently given by $F_o = \Phi_{fl}(T = 0)$ and $F_m = \Phi_{fl}(T \rightarrow \infty)$.

The above procedure yields fluorescence induction curves as well as the time dependence of the fraction of closed RCs, $C(T) = D(T)$. These are shown for the three parameter sets in Fig. 3, a and b, respectively. Data sets no. 1 and 3 display a clear sigmoidicity in the fluorescence induction curve. For data set no. 2, the sigmoidicity is less pronounced. The sigmoidicity is typically found in real experiments and is predicted by other theories based on rate equations (26). The higher F_m level for parameter set no. 3 is due to the slower loss processes ($k_1^{-1} = 3.3$ ns) in comparison to no. 1 and 2 ($k_1^{-1} = 1$ ns). Experimental fluorescence induction curves usually display a less pronounced sigmoidicity than the theoretical ones. This discrepancy may be ascribed to the assumption made in the theory of an infinite number of connected PSUs. In reality, only a limited number of PSUs may be coupled excitonically.

The different parameter sets lead to marked differences in the time dependence of the closed states (Fig. 3 b). For comparison, a hypothetical exponential closure of RC, characteristic for separate units, is also shown (Fig. 3 b, *dashed line*). This latter curve has a steeper initial slope than any of the calculated ones for the exciton–radical pair equilibrium model. Whereas the exponential law relates to a quantum yield of 1, the other curves have quantum yields of 0.80, 0.60, and 0.89 (pa-

rameter sets no. 1, 2, and 3, respectively). As the fraction of closed reaction centers increases, the exponential law predicts smaller quantum yields since, in contrast to the lake model, longer living excitons left in isolated units with closed RCs cannot find units with open RCs (Fig. 3 *b*).

Correlation between the variable fluorescence and the fraction of closed RCs

Fluorescence induction curves are often evaluated in terms of the relation between the variable fluorescence and the fraction of closed RCs. This yields bent curves that are analyzed using an analytical formula including a "connection parameter" (2, 27, 28). The degree of bending is interpreted as a measure for connectivity of PSUs or the "escape probability" out of the trap.

As the above calculation yields the time development of fluorescence as well as of closed RCs (Fig. 3, *a* and *b*), it is easy to correlate both quantities with each other. The variable fluorescence, $F_v(T)$, and the normalized variable fluorescence, $F_{v,n}(T)$, are defined as:

$$F_v(T) = \Phi_{fl}(T) - F_o, \tag{5a}$$

$$F_{v,n}(T) = \frac{F_v(T)}{F_m - F_o}. \tag{5b}$$

The variable fluorescence, $F_v(T \rightarrow \infty)$, shall be denoted in the following as F_v.

Fig. 3 *c* shows the relation between the normalized variable fluorescence and the fraction of closed RCs for the three parameter sets listed in Table 1. All three curves display different degrees of bending and, consequently, would be assigned different connection parameters in conventional induction analysis.

Correlation between the complementary area and the fraction of closed RCs

Another often used correlation in the evaluation of fluorescence induction curves is the relation between the area above a fluorescence induction curve (= complementary area) and the fraction of closed RCs. Both quantities are thought to be proportional to each other (1, 2). The proportionality has been demonstrated experimentally (29). It also has been derived from a simpler set of ODEs by Malkin and Kok (30) and by Murata et al. (31), who called the integral the "work integral." In other reports the complementary area normalized to the variable fluorescence was assumed to show this proportionality (30, 32, 33). The present calculations based on a physically interpretable molecular model allow for detailed examination of these conjectures.

The time dependence of the complementary area, $F_a(T)$, is defined as:

$$F_a(T) = \int_0^T (F_m - \Phi_{fl}(T))\, dT, \tag{6a}$$

and when normalized as:

$$F_{a,n}(T) = F_a(T)/F_a(T \rightarrow \infty). \tag{6b}$$

The total complementary area shall be defined as $F_a = F_a(T \rightarrow \infty)$.

Taking the three parameter sets listed in Table 1, the normalized complementary area is found to be strictly proportional to the fraction of closed RCs (Fig. 3 *d;* see also Figs. 4 *d*, 5 *d*, and 6 *d*). However, the nonnormalized values for the total complementary area, F_a, strongly may depend on the chosen rate constants (inset in Fig. 3 *a;* Table 1; see also Figs. 4 *a*, 5 *a*, and 6 *a*). The same applies to the complementary area normalized to the variable fluorescence, F_a/F_v (inset in Fig. 3 *a;* Table 1; see also Figs. 4 *a*, 5 *a*, and 6 *a*).

In summary, the proposed linear relationships hold only within one and the same fluorescence induction curve but not when fluorescence induction curves obtained in different experiments are compared.

Influence of the trapping time

The influence of the trapping time of open RCs was studied for $k_t = (0.3\ \text{ns})^{-1}$, $(0.5\ \text{ns})^{-1}$, and $(0.7\ \text{ns})^{-1}$ using parameter set no. 3. The corresponding fluorescence induction curves, time dependence of closed RCs, normalized variable fluorescence, and normalized complementary area versus the fraction of closed RCs are shown in Fig. 4, *a–d*, respectively.

Fig. 4 *a* shows that F_o increases with increasing trapping time, whereas F_m remains unaffected. If in closed RCs there is no other path for the radical pair to deactivate than to back react to the excited state, then F_m is independent of the parameters k_t^{red} and k_{-1}^{red}. This point has already been formulated before (34).

The shorter the trapping time, the faster is the fluorescence rise and the faster the closing of RCs (Fig. 4, *a* and *b*). The complementary area, F_a, and the complementary area normalized to the variable fluorescence, F_a/F_v, are rather insensitive to this parameter (inset in Fig. 4 *a*). The normalized variable fluorescence shows different curvatures (Fig. 4 *c*) and the normalized complementary area is proportional to the fraction of closed RCs (Fig. 4 *d*).

Influence of loss processes

The influence of losses in the antenna was studied for $k_l = (3\ \text{ns})^{-1}$, $(2\ \text{ns})^{-1}$, and $(1\ \text{ns})^{-1}$ using parameter set no. 3. The corresponding fluorescence induction curves, time dependence of closed RCs, normalized variable fluorescence, and normalized complementary area versus the fraction of closed RCs are shown in Fig. 5, *a–d*, respectively.

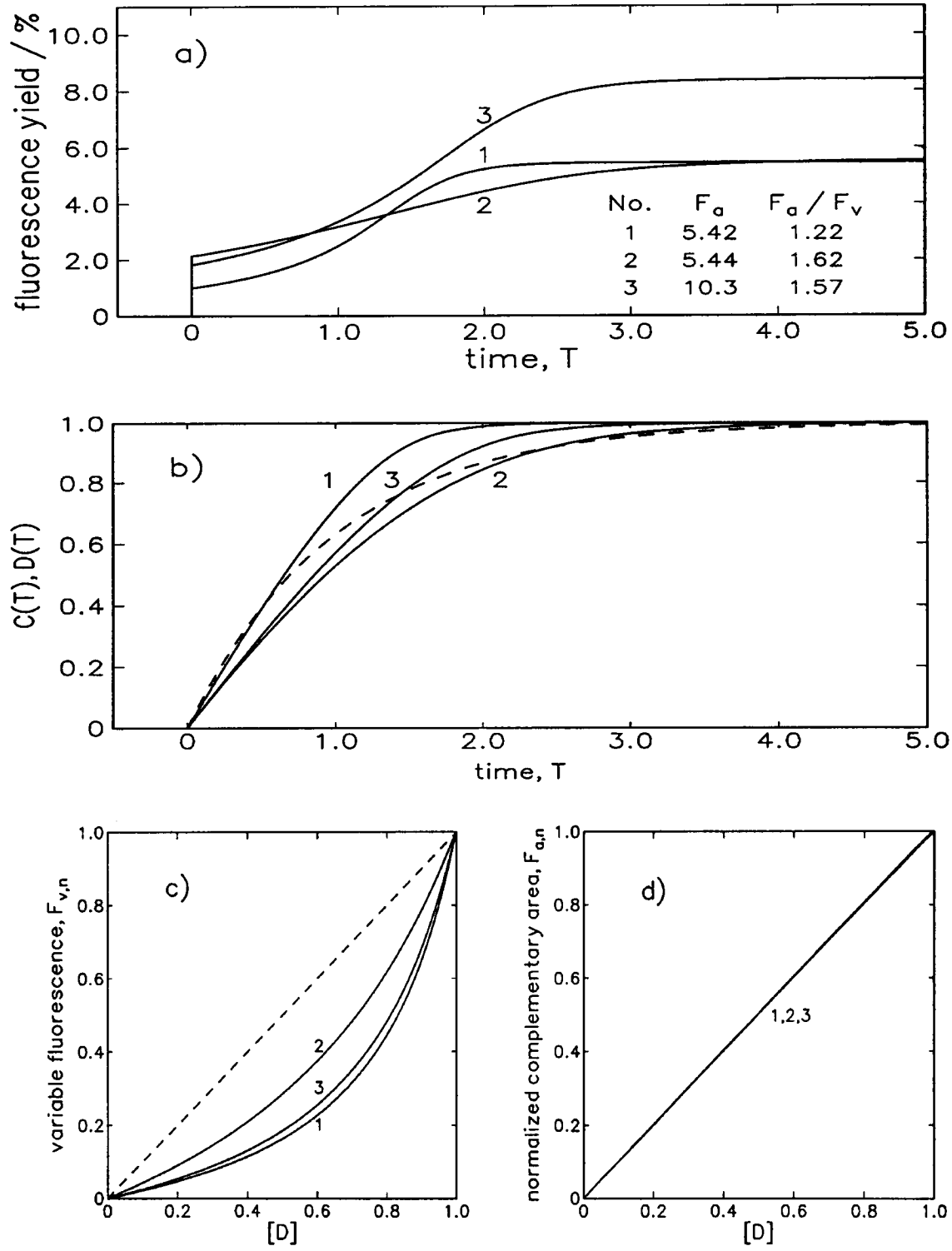

FIGURE 3 (*a*) Time course of the fluorescence yield (= fluorescence induction curves) calculated for the parameter sets no. 1, 2, and 3 (defined in Table 1). (*b*) Time course of the fraction of closed reaction centers, either *C* or *D*. (*c*) Relation between the normalized variable fluorescence, $F_{v,n}$, and the fraction of closed reaction centers, *D*, for the parameter sets no. 1, 2, and 3. (*d*) Relation between the normalized complementary area above the fluorescence induction curve, $F_{a,n}$, and the fraction of closed reaction centers, *D*.

As can be expected, faster decay pathways cause F_m to decrease more strongly than F_o (Fig. 5 *a*). The faster the loss processes, the slower the fluorescence rise and the slower the closing of RCs (Fig. 5, *a* and *b*). The complementary area, F_a, and the complementary area normalized to the variable fluorescence, F_a/F_v, display a significant sensitivity to this parameter (inset in Fig. 5 *a*). The normalized variable fluorescence shows different curva-

tures (Fig. 5 *c*), and the normalized complementary area is proportional to the fraction of closed RCs (Fig. 5 *d*).

Influence of losses of the radical pair P^+H^- to the ground state

There are strong arguments for including a decay path of the radical pair into a photochemically inactive state (either a triplet state, a relaxed radical pair state, or the ground state) (35, 36). It should be mentioned that decay paths were not explicitly separated in similar schemes published before (6–9, 37). A rate constant of the overall losses that is smaller in the open than in the closed state indicates whether losses from the radical pair state are significant. In cases where Q_A^- is directly measured (e.g., photovoltage measurements), this relaxation rate is experimentally well accessible. Nonetheless, it is possible to estimate this parameter also from time-resolved fluorescence decay measurements. Recently, it was quoted to be k_r^{-1} = 1–2 ns (20).

The influence of losses of the radical pair was examined for $k_r = (100\ \text{ns})^{-1}, (4\ \text{ns})^{-1}, (2\ \text{ns})^{-1}$, and $(1\ \text{ns})^{-1}$ using parameter set no. 3. The corresponding fluorescence induction curves, time dependence of closed RCs, normalized variable fluorescence, and normalized complementary area versus the fraction of closed RCs are shown in Fig. 6, *a–d*, respectively.

The influence of k_r on F_o is small due to the short lifetime of the radical pair in open RC. Its influence on F_m is more marked since in closed RCs the radical pair opens a new decay path for the excitons to the ground state (Fig. 6 *a*). The more pronounced this loss process, the slower the fluorescence rise and the slower the closing of RCs (Fig. 6, *a* and *b*). Both the complementary area, F_a, and the complementary area normalized to the variable fluorescence, F_a/F_v, are sensitive to this parameter (inset in Fig. 6 *a*). The normalized variable fluorescence shows slightly different curvatures (Fig. 6 *c*), and the normalized complementary area is proportional to the fraction of closed RCs (Fig. 6 *d*).

Time dependence

In Fig. 7 *a* the time courses of closed RCs, $D(T)$, the variable fluorescence, $F_{v,n}(T)$, and the complementary area, $F_{a,n}(T)$, are plotted semilogarithmically for the parameter set no. 3. It is obvious that none of these quantities obeys an exponential law (Fig. 7 *a, dotted straight line*).

Quenching by artificial quenchers

Artificial fluorescence quenchers like *m*-dinitrobenzene (DNB) are a useful tool in the study of antenna pigment organization in photosynthetic systems or trapping times (38, 39). The data evaluation usually yield straight lines in Stern–Volmer plots, in which the reciprocal fluorescence yield is plotted versus the concentration of the quenching substance, Q. In this study we wanted to test whether the exciton–radical pair equilibrium model (Fig. 1) predicts straight lines and whether quantitative agreement with published data can be achieved.

For this purpose a further deactivation path for the excited state was introduced with a quenching rate constant, k_q. This adds a term $-k_qQz$ to the first equation of the set of ODEs (Fig. 1, *bottom*):

$$1.\ dz/dt = \cdots - k_qQz \cdots$$

The corresponding normalized fluorescence yield was calculated viz:

$$F_n(Q) = \frac{\Phi_{fl,n}(Q)}{\Phi_{fl,n}(Q \to 0)}. \qquad (7)$$

Both the quenching rate constant, $k_q = (0.37\ \text{ns})^{-1}$, and the concentration scaling of quencher per PSU were chosen following Kischkoweit et al. (39). Stern–Volmer plots for F_m and F_o conditions are shown in Fig. 7 *b*, using parameter sets no. 1, 2, and 3. All of them, as well as the choice of other parameters, yielded straight Stern–Volmer lines. The slopes of parameter set no. 3 compare reasonably well with published data (39), indicating that these parameters and those in reference 39 are reasonably well determined.

It should be noted that the effect of artificial quenchers is formally equivalent to an altered rate constant for losses (see above). Therefore, in studies using quenching substances, the assumptions of invariability of the complementary area and of the normalized complementary area are not correct.

Fluorescence contribution from PS I

When comparing the fluorescence yield calculated here for PS II with experimental data, one should be aware of the contribution of fluorescence from PS I. To estimate this, we calculated the relative fluorescence yield of PS I using a trapping rate constant of k_t^{-1} = 110 ps and assuming irreversible trapping ($k_{-1} \to 0$). If the rate constant for losses is assumed to be k_l^{-1} = 2 ns and if the PS II fluorescence yield is set to 100%, then the contribution from PS I is ~25%. Hence, in experimental fluorescence induction curves ~20% of the F_o level should be subtracted from the fluorescence induction curves to obtain pure PS II induction curves. The 20% PS I fluorescence may be viewed as a "dead" component. This correction results in higher F_m/F_o ratios.

DISCUSSION

In the present work, "theoretical" fluorescence induction curves were calculated, solving a set of ODEs describing the primary photophysical and photochemical events in PS II by an exciton–radical pair equilibrium. This allowed us for the first time to correlate quantities derived from the shape of fluorescence induction curves with molecular rate constants as well as to inspect their

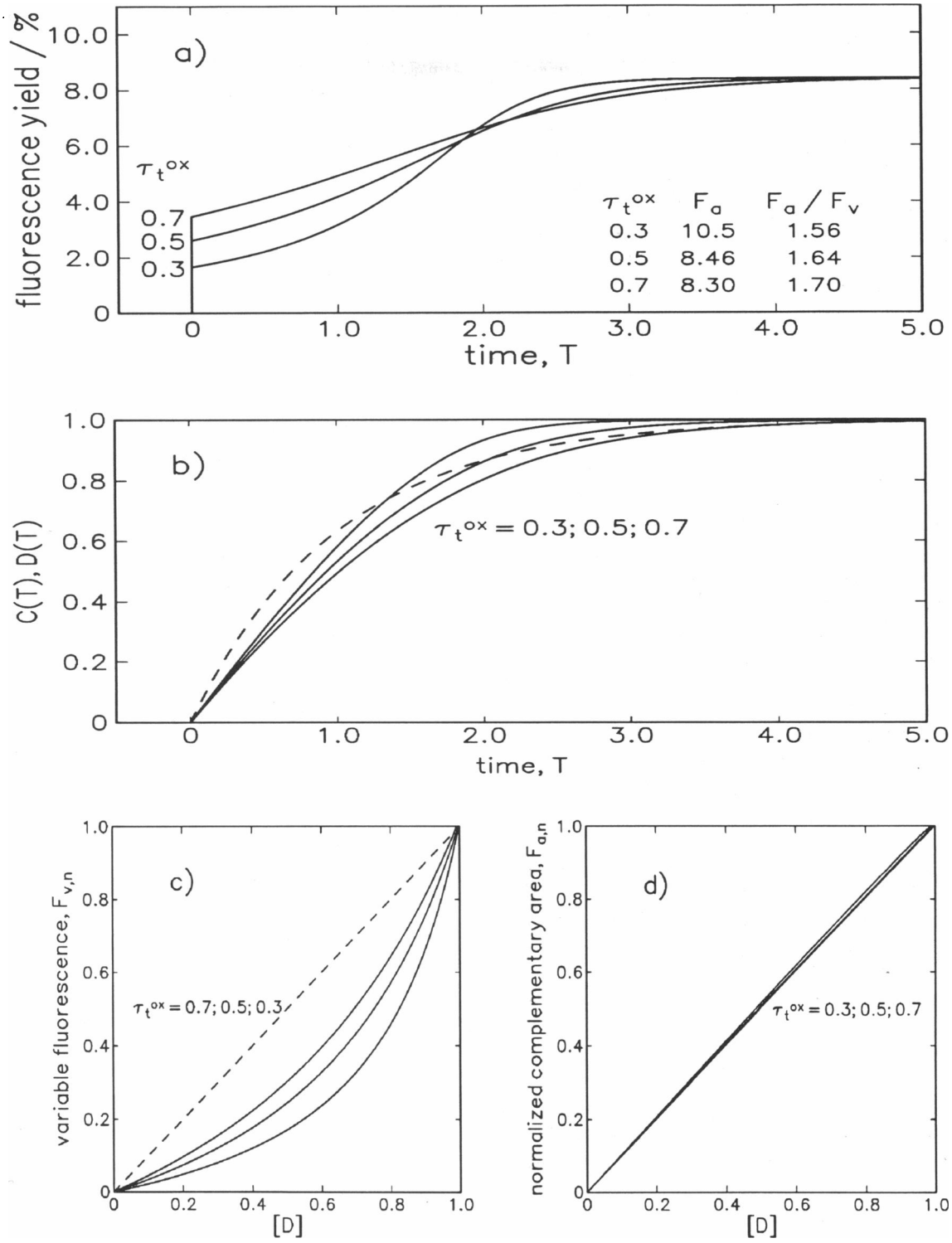

FIGURE 4 Influence of the trapping time rate constant of open RCs. (*a*) Fluorescence induction curves calculated for the parameter set no. 3. (*b*) Time course of the fraction of closed reaction centers, either *C* or *D*. (*c*) Relation between the normalized variable fluorescence, $F_{v,n}$, and the fraction of closed reaction centers, *D*. (*d*) Relation between the normalized complementary area above the fluorescence induction curve, $F_{a,n}$, and the fraction of closed reaction centers, *D*.

interrelations. Three basic assumptions were made: first, a trap-limited energy conversion; second, a perfect connectivity in the functional organization of antenna pigments, i.e., excitation energy can move freely among all PSUs; and third, homogeneity with respect to RC photochemistry and antenna size.

A great number of publications deal with similar theoretical treatments of fluorescence induction phenomena,

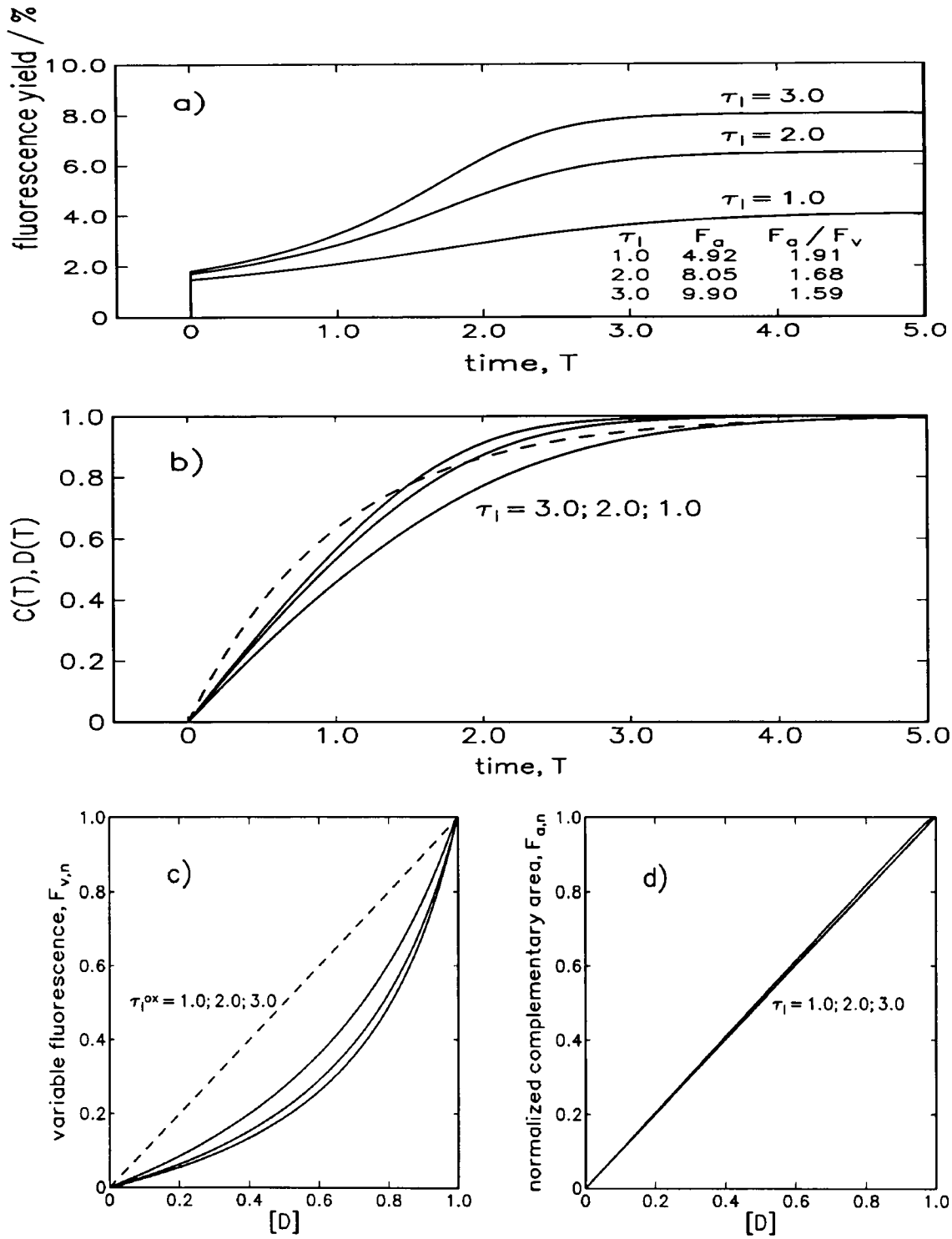

FIGURE 5 Influence of the rate constant of loss processes in the antenna. (*a*) Fluorescence induction curves calculated for the parameter set no. 3. (*b*) Time course of the fraction of closed reaction centers, either *C* or *D*. (*c*) Relation between the normalized variable fluorescence, $F_{v,n}$, and the fraction of closed reaction centers, *D*. (*d*) Relation between the normalized complementary area above the fluorescence induction curve, $F_{a,n}$, and the fraction of closed reaction centers, *D*.

aiming at providing a quantitative correlation between theoretically derived parameters and experimentally accessible variables (26, 30, 31, 41–44). Some of these studies aim at distinguishing between different organizations of PSUs with respect to the degree of energy transfer between the units (26, 41, 44). Several of these results are at variance with those derived in the present study. Without going too deeply into the details, one can in

general ascribe the discrepancies to different assumptions and concepts about the primary PS II photochemistry. To give an example, for decades it was uncertain whether energy conversion is diffusion or trap limited (for discussion see reference 45). To give another example, F_o is mostly thought to originate from ". . . fluorescence emitted from the bulk chlorophyll before the excitation energy is trapped by the reaction centers.", whereas ". . . F_m represents, in addition, the fluorescence which results from the excitation energy being transferred back from the closed reaction centers to the bulk chlorophyll" (26). This picture leads to the introduction of parameters accounting for "trapping" and "detrapping" and the creation of the term "escape probability" (21, 34). This is in contrast to the present treatment that assumes both the F_o fluorescence and the F_m fluorescence to originate from the reversibility of radical pair formation (Fig. 1). In our picture all parameters have clear physical meanings.

The following part of the discussion covers the sigmoidal shape of fluorescence induction curves and the absolute values for F_o and F_m. Furthermore, we shall discuss the particular relation between the fraction of closed RC and the variable fluorescence, the complementary area, as well as the time dependence of variable fluorescence and the complementary area. In the first parts of the discussion, a lake model organization of the antenna system is assumed, whereas in the last section we discuss whether it is possible to distinguish different antenna organizations by fluorescence induction analysis.

Sigmoidal shape of fluorescence induction curves

An obvious difference between our calculated fluorescence induction curves and experimental ones (e.g., 39) is the much more pronounced sigmoidicity in all theoretical curves with $F_m/F_o > 2$. The sigmoidicity is currently thought to be the main indicator for cooperation between PS II units (29). We believe that the less pronounced sigmoidicity in experimental curves is due to a limited energy transfer between some but not all PSUs (46, 47). A clarification of this point would require a more sophisticated theoretical approach, again being based on the exciton–radical pair equilibrium model but taking into account a restricted energy transfer and heterogeneous PS II populations.

Absolute values of F_o and F_m

In most experimental studies on fluorescence induction, relative or normalized scales are used. This principally represents a loss of valuable information, since the knowledge of the fluorescence quantum yields narrows down the possible ranges of rate constants. Energy transfer to other quenching centers in the photosynthetic membrane, as for example to PS I, may be inferred from known rate constants for the primary photochemistry of PS II and corresponding absolute quantum yields ("spill-over") (48). For open RCs, parameter sets no. 2 and 3 predict a $\approx$2% fluorescence yield. This value is close to an earlier estimated one (49).

Variable fluorescence

The variable fluorescence, F_v, divided by F_m is often taken as an index of the maximum yield of photochemistry (e.g., 26, 44). If this is true, then within the framework of the exciton–radical pair equilibrium model, the quantity $(F_v/F_m)/\Phi_p$ should be a constant. Calculating this ratio for the three parameter sets (Table 1), one obtains 0.653, 0.367, and 0.696, respectively. Because these numbers deviate strongly, the above assumed correlation can hardly be maintained.

Complementary area

According to our present calculations, the growth of the complementary area with time, $F_a(T)$, is strictly proportional to the concentration of Q_A^-. This is in perfect agreement with experimental data (50).

However, this internal proportionality should not be confused with an external proportionality between the total complementary area, F_a, and the number of redox equivalents transferred to the acceptor side as has been proposed previously (30, 31). Such a proportionality does not exist, as the values for F_a differ strongly when the rate constants are changed, although there is only one electron being transferred in our theoretical calculations (see insets of Figs. 3–6). Also, when the complementary area is normalized to the variable fluorescence, F_a/F_v (Table 1) is not an accurate indicator of the number of electron acceptors (33). Hence, to deduce from F_a measurements that oxidation of the non-heme iron located between Q_A and Q_B allows exactly one more electron to be taken up may be questionable. The chemical oxidation of Fe^{++} is likely to change the rate constants as much as does the reduction of Q_A (33). It follows that the cause of experimentally observed changes in F_a is difficult to assess.

In the past, an inverse proportionality between the complementary area, normalized to the variable fluorescence, and the photosynthetic quantum yield has been proposed (28, 32). Also this relation cannot be confirmed, as $(F_a/F_v)\cdot\Phi_p$ adopts values of 0.976, 0.842, and 1.400 taking parameter sets no. 1, 2, 3, respectively (Table 1). The same argument would apply to the quantity $(F_a/F_v)\cdot\Phi_m$.

Time dependence of variable fluorescence and complementary area

Fluorescence induction curves are often analyzed using semilogarithmic plots. Fig. 7 *a* shows that neither the fraction of closed RC nor the variable fluorescence nor the complementary area displays straight lines in a semilogarithmic plot. Therefore, the frequently practiced

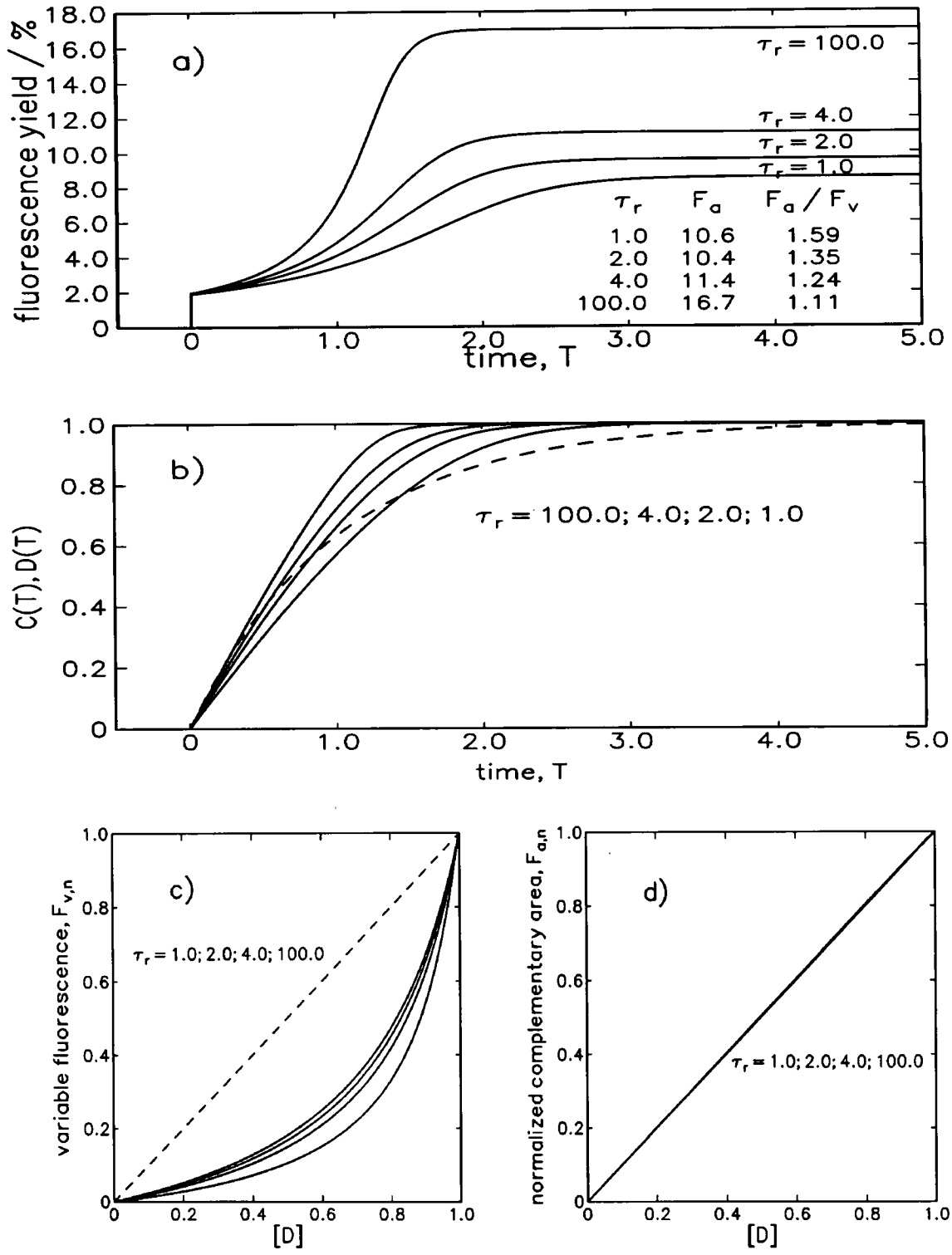

FIGURE 6 Influence of the rate constant for the decay of the radical pair into the ground state. (*a*) Fluorescence induction curves calculated for the parameter set no. 3. (*b*) Time course of the fraction of closed reaction centers, either *C* or *D*. (*c*) Relation between the normalized variable fluorescence, $F_{v,n}$, and the fraction of closed reaction centers, *D*. (*d*) Relation between the normalized complementary area above the fluorescence induction curve, $F_{a,n}$, and the fraction of closed reaction centers, *D*.

analysis of fluorescence induction curves by semilogarithmic plots is not meaningful at all and little suited for the determination of rate constants from the slopes at zero time (51, 52). In the case of heterogeneous photosystems, it might be conceivable to separate photosystems with large antenna sizes from those with smaller

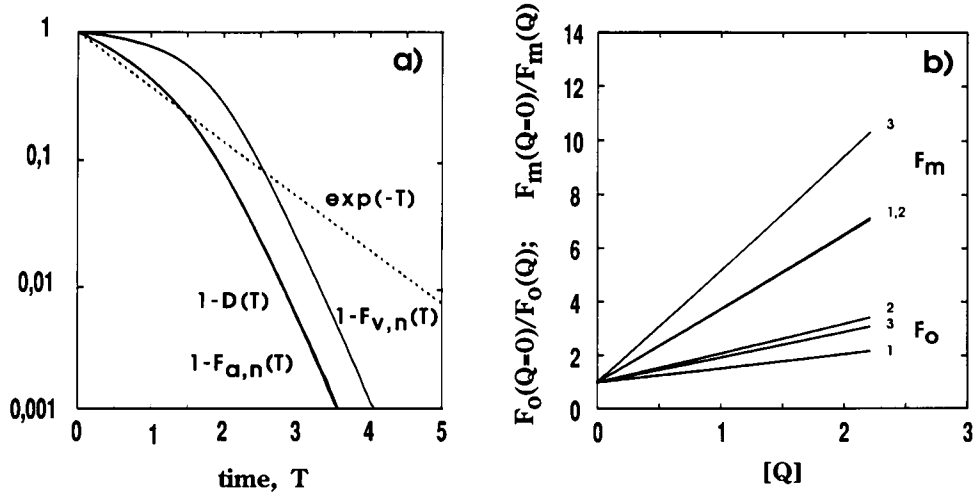

FIGURE 7 (*a*) Semilogarithmic plot of the time courses of the normalized variable fluorescence, $(1 - F_{v,n})$, the normalized complementary area above the fluorescence induction curve, $(1 - F_{a,n})$, the closure of reaction centers, $(1\ D)$, calculated for parameter set no. 3. Furthermore, the exponential kinetics, $\exp(-z)$, is graphed as a dotted line. (*b*) Calculated Stern–Volmer plots of fluorescence quenching at F_m and F_o conditions by the addition of an artificial quenching substance like DNB with a quenching rate constant of $k_q^{-1} = 0.37$ ns (39). The concentration of the quencher is expressed according to Fig. 1 by the dimensionless number Q, i.e., quenchers per PSU. The calculation was carried out with parameter set no. 3. To correlate Q with the DNB concentration given in millimolars, we used Eq. 2 in Kischkoweit et al. (39) and the numerical values reported therein (39).

ones (e.g., PS II_α/PS II_β) by subtraction on a semilogarithmic plot, provided the latter are organized as separate units and therefore display exponential kinetics dominating at long times. However, this latter assumption is a matter of debate (51, 52).

Different antenna organizations

The curvature in plots of the normalized variable fluorescence versus the fraction of closed RC is occasionally understood as a measure for the degree of connectivity between PS II units. In several theories, formulas are derived for this relation that contain the so-called "connection parameter, p" (27, 28, 53, 54; for review see 2) and that allow good fits to experimental curves like those in Figs. 3 *c*, 4 *c*, 5 *c*, and 6 *c*. The correct interpretation of this parameter is that p ". . . describes two distinct processes, an inter-PSU excitation propagation and an inter-center competition for excitation capture" (28). In practice, p adopts values between 0.5 and 0.7.

Fig. 3 *c* shows that the relation between the variable fluorescence and the fraction of closed RCs displays different degrees of bending on changing the molecular rate constants. Hence, it has to be concluded that the degree of bending cannot be a measure for the mean free path (travel distance) of excitons (e.g., domain size) since a perfect connectivity was assumed throughout our calculations. A similar argument already has been presented by Valkunas et al. (55). In this context it is worth mentioning that a sigmoidal fluorescence increase can also occur in a separate unit model (55, 56).

Recently, in a random-walk model that describes exciton dynamics in a domain, a linear dependence of the reciprocal fluorescence yield, and the fraction of closed RCs was derived for the limiting case of infinitely large domains (57). Smaller domain sizes cause positive curvatures (46, 57). The exciton–radical pair equilibrium model predicts for all three parameter sets linear relations (Fig. 8). Hence, if the fraction of closed RCs can experimentally be determined with high precision, the evaluation of such plots does allow conclusions on the antenna organization.

CONCLUSIONS

Innumerable factors are known to influence and complicate the fluorescence yield in PS II. Among those are the degree of stacking, membrane potential, membrane energetization, divalent cations, pH, S states of the water splitting complex, redox state of the non-heme iron, and finally the α-,β-heterogeneity. None of those has been considered here. Nonetheless, the fluorescence phenomena under evaluation in this study vary strongly and in a complex manner just by changing some molecular rate constants in a quite simple reaction scheme. It thus appears that data on fluorescence induction phenomena frequently has been subjected to mis- and overinterpretation. Serious complications in the interpretation of fluorescence yield changes have been recognized before (4).

We can draw six explicit conclusions that apply to PS II with blocked e^- transfer behind Q_A.

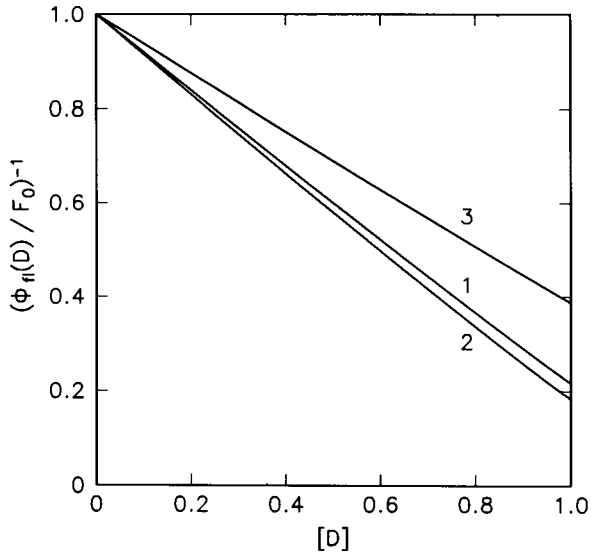

FIGURE 8 Plot of the reciprocal normalized fluorescence yield, $(\Phi_{fl}(D)/F_0)^{-1}$, versus the fraction of closed reaction centers, D, using parameter set no. 1–3 (Table 1).

(a) There is proportionality between the complementary area and the fraction of closed RCs only for one given experimental condition.

(b) There is no proportionality between the complementary area and the number of electrons flowing to the acceptor site, since in our model calculations the number of electrons was invariably set to one.

(c) None of the fluorescence quantities yields a straight line in semilogarithmic plots versus time.

(d) It is not possible to determine the degree of connectivity between PSUs or the domain size from the curvature of the variable fluorescence plotted versus the fraction of closed reaction centers, since even assuming a perfect lake-model the curvature will strongly depend on rate constants.

(e) Fluorescence induction curves obtained under different experimental conditions are hard to interpret since it proves difficult to distinguish between altered rate constants and an altered degree of connectivity.

(f) The assumption of perfectly connected PSUs is probably not given in real systems.

(g) Heterogeneity in PS II represents a serious impediment to theoretical and experimental analysis.

We thank Prof. Dr. W. Junge for general support and laboratory facilities, Dr. N. Geacintov for helpful discussions, and Dipl. Biol. A. Pokorny for critical reading of the manuscript.

This work was financially supported by the Deutsche Forschungsgemeinschaft (Sonderforschungsbereich 171, TP-A1, and TR 129/4-1).

Received for publication 18 August 1992 and in final form 25 November 1992.

REFERENCES

1. Lavorel, J., J. Breton, and M. Lutz. 1986. Methodological principles of measurements of light emitted by photosynthetic systems. *In* Light Emission by Plants and Bacteria. Govindjee, J. Amesz, and D. C. Fork, editors. Academic Press, Inc., Orlando/San Diego. 57–98.
2. Lavorel, J., and A.-L. Etienne. 1977. In vivo chlorophyll fluorescence. *In* Topics in Photosynthesis. Vol. 2. Primary Processes of Photosynthesis. J. Barber, editor. Elsevier/North-Holland Biomedical Press, 203–268.
3. Geacintov, N. E., and J. Breton. 1987. Energy transfer and fluorescence mechanisms in photosynthetic membranes. *Crit. Rev. Plant Sci.* 5:1–44.
4. van Gorkom, H. J. 1986. Fluorescence measurements in the study of photosystem II electron transport. *In* Light Emission by Plants and Bacteria. Govindjee, J. Amesz, and D. C. Fork, editors. Academic Press, Inc., Orlando/San Diego. 267–289.
5. van Gorkom, H. J. 1985. Electron transfer in photosystem II. *Photosynth. Res.* 6:97–112.
6. Schatz, G. H., and A. R. Holzwarth. 1986. Mechanisms of chlorophyll fluorescence revisited: prompt or delayed emission from photosystem II with closed reaction centers? *Photosynth. Res.* 10:309–318.
7. Schatz, G. H., H. Brock, and A. R. Holzwarth. 1987. Picosecond kinetics of fluorescence and absorbance changes in photosystem II particles excited at low photon density. *Proc. Natl. Acad. Sci. USA.* 84:8414–8418.
8. Schatz, G. H., H. Brock, and A. R. Holzwarth. 1988. Kinetic and energetic model for the primary processes in photosystem II. *Biophys. J.* 54:397–405.
9. Leibl, W., J. Breton, J. Deprez, and H.-W. Trissl. 1989. Photoelectric study on the kinetics of trapping and charge stabilization in oriented PS II membranes. *Photosynth. Res.* 22:257–275.
10. Holzwarth, A. R. 1991. Excited state kinetics in chlorophyll systems and its relationship to the functional organization of the photosystems. *In* The Chlorophylls. H. Scheer, editor. CRC Press, Boca Raton/Ann Arbor. 1125–1151.
11. Wasielewski, M. R., D. G. Johnson, M. Seibert, and Govindjee. 1989. Determination of the primary charge separation rate in isolated photosystem II reaction centers with 500-fs time resolution. *Proc. Natl. Acad. Sci. USA.* 86:524–528.
12. Roelofs, T. A., M. Gilbert, V. A. Shuvalov, and A. R. Holzwarth. 1991. Picosecond fluorescence kinetics of the D1-D2-cyt-b-559 photosystem II reaction center complex: energy transfer and primary charge separation processes. *Biochim. Biophys. Acta.* 1060:237–244.
13. Owens, T. G., S. P. Webb, L. J. Mets, R. S. Alberte, and G. R. Fleming. 1987. Antenna size dependence of fluorescence decay in the core antenna of photosystem I: estimates of charge separation and energy transfer rates. *Proc. Natl. Acad. Sci. USA.* 84:1532–1536.
14. Eads, D. D., E. W. Castner, R. S. Alberte, L. Mets, and G. R. Fleming. 1989. Direct observation of energy transfer in a photosynthetic membrane: chlorophyll b to chlorophyll a transfer in LHC. *J. Phys. Chem.* 93:8271–8275.
15. Hemelrijk, P. W., S. L. S. Kwa, R. van Grondelle, and J. P. Dekker. 1992. Spectroscopic properties of LHC-II, the main light-harvesting chlorophyll a/b protein complex from chloroplast membranes. *Biochim. Biophys. Acta.* 1098:159–166.
16. Owens, T. G., S. P. Webb, R. S. Alberte, L. J. Mets, and G. R. Fleming. 1988. Antenna structure and excitation dynamics in photosystem I. I. Studies of detergent-isolated photosystem I

preparations using time-resolved fluorescence analysis. *Biophys. J.* 53:733–745.

17. McCauley, S. W., E. Bittersmann, and A. R. Holzwarth. 1989. Time-resolved ultrafast blue-shifted fluorescence from pea chloroplasts. *FEBS (Fed. Eur. Biochem. Soc.) Lett.* 249:285–288.
18. Meiburg, R. F., H. J. van Gorkom, and R. J. van Dorssen. 1983. Excitation trapping and charge separation in photosystem II in the presence of an electric field. *Biochim. Biophys. Acta.* 724:352–358.
19. Keuper, H. J. K., and K. Sauer. 1989. Effect of photosystem II reaction center closure on nanosecond relaxation kinetics. *Photosynth. Res.* 20:85–103.
20. Roelofs, T. A., C.-H. Lee, and A. R. Holzwarth. 1992. Global target analysis of picosecond chlorophyll fluorescence kinetics from pea chloroplasts. A new approach to the characterization of the primary processes in photosystem II α- and β-units. *Biophys. J.* 61:1147–1163.
21. Ley, A. C., and D. Mauzerall. 1986. The extent of energy transfer among photosystem II reaction centers in *Chlorella. Biochim. Biophys. Acta.* 850:234–248.
22. Trissl, H.-W., J. Breton, J. Deprez, and W. Leibl. 1987. Primary electrogenic reactions of photosystem II as probed by the light-gradient method. *Biochim. Biophys. Acta.* 893:305–319.
23. Den Haan, G. A., J. T. Warden, and L. N. M. Duysens. 1973. Kinetics of the fluorescence yield of chlorophyll *a* in spinach chloroplasts at liquid nitrogen temperature during and following a 16 μs flash. *Biochim. Biophys. Acta.* 325:120–125.
24. Jursinic, P. A., and Govindjee. 1977. The rise in chlorophyll *a* fluorescence yield and decay in delayed light emission in Tris-washed chloroplasts in the 6-100 μs time range after an excitation flash. *Biochim. Biophys. Acta.* 461:253–267.
25. Melis, A., and J. M. Anderson. 1983. Structural and functional organization of the photosystems in spinach chloroplasts. Antenna size, relative electron-transport capacity, and chlorophyll composition. *Biochim. Biophys. Acta.* 724:473–484.
26. Butler, W. L., and M. Kitajima. 1975. Fluorescence quenching in photosystem II of chloroplasts. *Biochim. Biophys. Acta.* 376:116–125.
27. Joliot, P., and A. Joliot. 1964. Études cinétique de la réaction photochimique libérant l'oxygene au cours de la photosynthese. *C. R. Acad. Sci. Paris.* 258:4622–4625.
28. Paillotin, G. 1976. Movement of excitations in the photosynthetic domains of photosystem II. *J. Theor. Biol.* 58:237–252.
29. Bennoun, P., and Y.-S. Li. 1973. New results on the mode of action of 3,-(3,4-dichloro-phenyl)-1,1-dimethyl-urea in spinach chloroplasts. *Biochim. Biophys. Acta.* 292:162–168.
30. Malkin, S., and B. Kok. 1966. Fluorescence induction studies in isolated chloroplasts. I. Number of components involved in the reaction and quantum yields. *Biochim. Biophys. Acta.* 126:413–432.
31. Murata, N., M. Nishimura, and A. Takamiya. 1966. Fluorescence of chlorophyll in photosynthetic systems. II. Induction of fluorescence in isolated spinach chloroplasts. *Biochim. Biophys. Acta.* 120:23–33.
32. Etienne, A.-L., C. Lemasson, and J. Lavorel. 1974. Quenching de la chlorophylle in vivo par le *m*-dinitrobenzene. *Biochim. Biophys. Acta.* 333:288–300.
33. Ikegami, I., and S. Katoh. 1973. Studies on chlorophyll fluorescence in chloroplasts. II. Effect of ferricyanide on the induction of fluorescence in the presence of 3-(3,4-dichlorophenyl)-1,1-dimethylurea. *Plant Cell Physiol.* 14:829–836.
34. Butler, W. L. 1984. Exiton transfer out of open photosystem II reaction centers. *Photochem. Photobiol.* 40:513–518.
35. Schlodder, E., and K. Brettel. 1988. Primary charge separation in closed photosystem II with a lifetime of 11 ns. Flash-absorption spectroscopy with oxygen-evolving photosystem II complexes from *Synechococcus. Biochim. Biophys. Acta.* 933:22–34.
36. Roelofs, T. A., and A. R. Holzwarth. 1990. In search of a putative long-lived relaxed radical pair state in closed photosystem II. Kinetic modeling of picosecond fluorescence data. *Biophys. J.* 57:1141–1153.
37. Källebring, B., and Ö. Hansson. 1991. A theoretical study of the effect of charge recombination on the transfer and trapping of excitation energy in photosynthesis. *Chem. Phys.* 149:361–372.
38. Sonneveld, A., H. Rademaker, and L. N. M. Duysens. 1980. Transfer and trapping of excitation energy in photosystem II as studied by chlorophyll *a* fluorescence quenching by dinitrobenzene and carotenoid triplet. The matrix model. *Biochim. Biophys. Acta.* 593:272–289.
39. Kischkoweit, C., W. Leibl, and H.-W. Trissl. 1988. Theoretical and experimental study of trapping times and antenna organization in pea chloroplasts by means of the artificial fluorescence quencher *m*-dinitrobenzene. *Biochim. Biophys. Acta.* 933:276–287.
40. Paillotin, G., N. E. Geacintov, and J. Breton. A master equation theory of fluorescence induction, photochemical yield, and singlet-triplet exciton quenching in photosynthetic systems. *Biophys. J.* 44:65–77.
41. Clayton, R. K. 1967. An analysis of the relations between fluorescence and photochemistry during photosynthesis. *J. Theor. Biol.* 14:173–186.
42. Lavorel, J., and P. Joliot. 1972. A connected model of the photosynthetic unit. *Biophys. J.* 12:815–831.
43. Kitajima, M., and W. L. Butler. 1975. Quenching of chlorophyll fluorescence and primary photochemistry in chloroplasts by dibromothymoquinone. *Biochim. Biophys. Acta.* 376:105–115.
44. Hipkins, M. F. 1978. Kinetic analysis of the chlorophyll fluorescence inductions from chloroplasts blocked with 3-(3,4,-dichlorophenyl)-1,1-dimethylurea. *Biochim. Biophys. Acta.* 502: 514–523.
45. Beauregard, M., I. Martin, and A. R. Holzwarth. 1991. Kinetic modelling of exciton migration in photosynthetic systems. 1. Effects of pigment heterogeneity and antenna topography on exciton kinetics and charge separation yields. *Biochim. Biophys. Acta.* 1060:271–283.
46. van Grondelle, R. 1985. Excitation energy transfer, trapping and annihilation in photosynthetic systems. *Biochim. Biophys. Acta.* 811:147–195.
47. Renger, G., and A. Schulze. 1985. Quantitative analysis of fluorescence induction curves in isolated spinach chloroplasts. *Photobiochem. Photobiophys.* 9:79–87.
48. Malkin, S., and D. C. Fork. 1981. Photosynthetic units of sun and shade plants. *Plant Physiol. (Bethesda).* 67:580–583.
49. Duysens, L. N. M. 1979. Transfer and trapping of excitation energy in photosystem II. *In* Chlorophyll Organization and Energy Transfer in Photosynthesis. Ciba Foundation Symposium 61 (New Series). G. Wolstenholme and D. W. Fitzsimons, editors. Excerpta Medica, Amsterdam/New York. 323–340.
50. Melis, A., and L. N. M. Duysens. 1979. Biphasic energy conversion kinetics and absorbance difference spectra of photosystem II of chloroplasts. Evidence for two different photosystem II reaction centers. *Photochem. Photobiol.* 29:373–382.
51. Melis, A., and P. H. Homann. 1975. Kinetic analysis of the fluorescence induction in 3-(3,4-dichlorophenyl)-1,1-demethylurea poisoned chloroplasts. *Photochem. Photobiol.* 21:431–437.
52. McCauley, S., and A. Melis. 1987. Quantification of photosystem

II activity in spinach chloroplasts. Effect of artificial quinone acceptors. *Photochem. Photobiol.* 46:543–550.

53. Delosme, R., P. Joliot, and J. Lavorel. 1959. Sur la complémentarité de la fluorescence et de l'emission d'oxygène pendant la période d'induction de la photosynthèse. *C. R. Acad. Sci. Paris.* 249:1409–1411.
54. Butler, W. L. 1978. Energy distribution in the photochemical apparatus of photosynthesis. *Annu. Rev. Plant Physiol.* 29:345–378.
55. Valkunas, L. L., N. E. Geacintov, L. France, and J. Breton. 1991. The dependence of the shapes of fluorescence induction curves in chloroplasts on the duration of illumination pulses. *Biophys. J.* 59:397–408.
56. Lavorel, J. 1972. Modele d'unites photosynthetiques á trois etats. *C. R. Acad. Sci. Paris.* 274:2909–2912.
57. Den Hollander, W. T. F., J. G. C. Bakker, and R. van Grondelle. 1983. Trapping, loss and annihilation of excitations in a photosynthetic system. I. Theoretical aspects. *Biochim. Biophys. Acta.* 725:492–507.